Near-Unity Quantum Yields of Biexciton Emission from CdSe/CdS Nanocrystals Measured Using Single-Particle Spectroscopy

Y.-S. Park,[1,2] A. V. Malko,[4] J. Vela,[1,2,*] Y. Chen,[1,2,†] Y. Ghosh,[1,2] F. García-Santamaría,[1,‡] J. A. Hollingsworth,[1,2] V. I. Klimov,[1,3,§] and H. Htoon[1,2,‖]

[1]*Chemistry Division, Los Alamos National Laboratory, Los Alamos, New Mexico 87545, USA*
[2]*Center for Integrated Nanotechnologies, Los Alamos National Laboratory, Los Alamos, New Mexico 87545, USA*
[3]*Center for Advanced Solar Photophysics, Los Alamos National Laboratory, Los Alamos, New Mexico 87545, USA*
[4]*Department of Physics, The University of Texas at Dallas, Richardson, Texas 75080, USA*

(Received 20 December 2010; published 3 May 2011)

Biexciton photoluminescence (PL) quantum yields (Q_{2X}) of individual CdSe/CdS core-shell nanocrystal quantum dots with various shell thicknesses are derived from independent PL saturation and two-photon correlation measurements. We observe a near-unity Q_{2X} for some nanocrystals with an ultrathick 19-monolayer shell. High Q_{2X}'s are, however, not universal and vary widely among nominally identical nanocrystals indicating a significant dependence of Q_{2X} upon subtle structural differences. Interestingly, our measurements indicate that high Q_{2X}'s are not required to achieve complete suppression of PL intensity fluctuations in individual nanocrystals.

DOI: 10.1103/PhysRevLett.106.187401 PACS numbers: 78.67.Bf, 73.21.La, 78.55.−m

Semiconductor nanocrystal quantum dots (NQDs) with near-perfect photoluminescence (PL) quantum yields (QYs) can be routinely synthesized using methods of colloidal chemistry [1,2]. However, these high QYs can only be obtained for single-exciton (1X) states. QYs of multiexcitons (Q_{mX}, $m > 1$) are, in contrast, very low ($< 10\%$) due to fast nonradiative Auger recombination [3–5]. High values of Q_{mX} are, however, essential for practical realization of NQD applications such as lasing [6] and generation of entangled photon pairs [7,8]. To this end, nanorods [9], nanowires [10], and inverted core-shell NQDs [11] have been investigated. They, however, have shown only a moderate suppression of Auger recombination arising primarily from increased spatial separation between carriers. More recently, strongly suppressed Auger decays were reported for alloyed CdZnSe/ZnSe [12] and CdTe/CdSe [13] core-shell NQDs as inferred from observations of reduced blinking [12] and efficient emission from multiexcitons [13] in single-dot studies.

A new type of core-shell NQD, in which 3–4 nm diameter CdSe cores are overcoated with a thick [> 10 monolayers (MLs)] CdS shell, has recently emerged as a promising nanostructure for realizing suppressed Auger recombination [14,15]. Initially, these NQDs [dubbed ''giant'' NQDs (GNQDs)] were reported to exhibit significantly suppressed blinking [14–16]. More recent studies also revealed signatures of suppression of Auger decay including efficient multiband amplified spontaneous emission [17], long biexciton (2X) recombination times that could not be explained by traditional scaling with NQD volume [17,18], and strong features due to charged excitons (trions) and multiexcitons in single-NQD PL spectra [19,20]. These observations are suggestive of high PL efficiencies of multiexcitons in these structures. However, so far, Q_{mX} in individual GNQDs has not been measured, and neither has the uniformity of Q_{mX} across a nanocrystal ensemble been analyzed.

Here, we address this issue by investigating the distribution of Q_{2X}'s in samples of nominally identical GNQDs using two independent single-dot spectroscopic techniques. We observe excellent agreement between the two methods over a wide range of the Q_{2X} values. We show that Q_{2X} of ~ 0.9 can be achieved in GNQDs with shell thickness >16 ML. However, the values of Q_{2X} exhibit a broad distribution indicating a strong influence of NQD internal structure on Q_{2X}. Significantly, even in the case of completely suppressed PL fluctuations (observed for all >16 ML dots), Q_{2X}'s and, hence, the degree of Auger decay suppression vary widely. This leads to an important conclusion: the suppression of PL fluctuations and the suppression of Auger decay are not necessarily related. This might imply that the thick shells of our GNQDs suppress PL fluctuations by either preventing photoionization or restraining random migration of long-lived charges if photoionization still takes place.

CdSe/CdS core-shell NQDs are synthesized via a modified successive ionic layer deposition procedure [14]. The NQDs are dispersed on a quartz substrate with a density of $\sim 0.01/\mu\text{m}^2$ and excited with 50 ps, 405 nm laser pulses through a 60X, 0.7 numerical aperature objective that is also used to collect PL. The laser repetition rates are selected to ensure complete relaxation of excitons between sequential pulses. The PL spectra are recorded with a cryogenically cooled charge-coupled device through a $1/3$ m spectrometer. For two-photon correlation measurements, we use a traditional setup comprising a 50:50 beam splitter and two single-photon Si detectors (350 ps time resolution). All studies are performed at room temperature.

We utilize two independent approaches to measure $Q_{m\mathrm{X}}$ in individual NQDs. In the first, we obtain $Q_{2\mathrm{X}}$ by analyzing the pump-intensity dependence of the spectrally integrated PL. We assume that upon photoexcitation the probability of finding an NQD in the N-exciton state is given by the Poisson distribution: $P(N,\langle N\rangle) = \langle N\rangle^N e^{-\langle N\rangle}/N!$, where $\langle N\rangle$ is the average NQD occupancy. This approach requires knowledge of the NQD absorption cross section (σ) and certain assumptions on the scaling of the radiative and the nonradiative recombination rates with N. We have also applied an independent method, in which $Q_{2\mathrm{X}}$ is derived from the second-order PL intensity correlation ($g^{(2)}$) measurements. This technique, which was recently applied to standard NQDs [21], yields the ratio of the $Q_{2\mathrm{X}}$ and single-exciton QY ($Q_{1\mathrm{X}}$) based on the relative amplitudes of the coincidence features in $g^{(2)}$ of the NQD under weak-excitation conditions. This approach is more direct as it does not rely on any of the aforementioned assumptions.

Figure 1(a) displays the pump-power dependence of the spectrally integrated PL of four NQDs with 4-, 7-, 16-, and 19-ML-thick CdS shells. For this plot, $\langle N\rangle$ is calculated using σ independently determined by assuming that it scales linearly with the NQD volume [22] (inset of Fig. 1 and supplemental material [23]). To compare different samples in the same plot, we normalize PL intensities assuming that at low pump levels ($\langle N\rangle < 0.5$) $Q_{1\mathrm{X}} = 1$

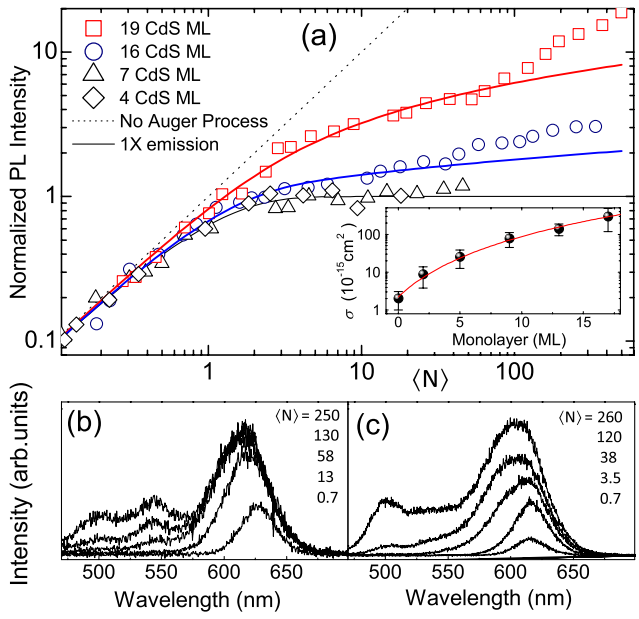

FIG. 1 (color online). (a) Pump-power dependence of the PL intensity for four single NQDs. Solid lines are the fits to the "PL-saturation" model which yield $Q_{2\mathrm{X}} \approx 0.14$ and 0.56 for 16- and 19-ML shell NQDs, respectively. Inset: NQD absorption cross sections plotted as a function of shell thickness. Pump-power-dependent PL spectra of (b) 16- and (c) 19-ML shell GNQDs showing the emergence of higher-energy emission bands (450–575 nm) at large $\langle N\rangle$.

for all dots. This assumption reduces the number of fitting parameters; the implications of a nonunity $Q_{1\mathrm{X}}$ are discussed later in this Letter and also in the supplemental material [23]. While normalized traces are similar at low pump intensities, the PL behavior becomes sample dependent when $\langle N\rangle > 1$ [Fig. 1(a)]. Specifically, normalized PL intensity (I) of the 4- and 7-ML samples reaches complete saturation, while that from the 16- and 19-ML shell dots still grows with $\langle N\rangle$. This increase occurs due to continuing growth of the band-edge PL as well as the development of new higher-energy bands [Figs. 1(b) and 1(c)], indicating enhanced $Q_{m\mathrm{X}}$'s values compared to thin-shell samples.

In order to quantitatively describe this behavior, we model I as $I = \sum_{N=1}^{\infty} P(N,\langle N\rangle) \sum_{m=1}^{N} Q_{m\mathrm{X}}$. In the case of $Q_{m\mathrm{X}}(m > 1) = 0$, I becomes $I = (1 - e^{-\langle N\rangle})$. This saturation curve [solid black line in Fig. 1(a)], which describes a typical behavior of standard dots, falls directly on top of the data points for NQDs with 4- and 7-ML shells. To describe a weak saturation behavior of the 16- and 19-ML shell GNQDs, we assume that radiative and nonradiative Auger decay rates of the m-exciton state ($k_{m\mathrm{X},R}$ and $k_{m\mathrm{X},NR}$, respectively) scale linearly with the number of available recombination pathways: $k_{m\mathrm{X},R} \propto m^2$ and $k_{m\mathrm{X},NR} \propto m^2(m-1)$ [24]. Under this assumption, an expression for $Q_{m\mathrm{X}}$ can be written as $Q_{m\mathrm{X}} = [1 + (m-1)A]^{-1}$; it contains a single adjustable parameter, $A = k_{2\mathrm{X},NR}/k_{2\mathrm{X},R}$, which defines the value of $Q_{2\mathrm{X}}$: $Q_{2\mathrm{X}} = (1 + A)^{-1}$.

We use this model to fit the PL-saturation data for 16- and 19-ML shell GNQDs up to $\langle N\rangle$ of $\sim$25 [Fig. 1(a)]. The fitting provides $Q_{2\mathrm{X}}$ of 0.14 ± 0.03 and 0.56 ± 0.04 for the 16- and 19-ML GNQDs, respectively. At very high pump intensities ($\langle N\rangle > 25$), the PL intensity takes an upward turn, which correlates with the emergence of high-energy emission bands attributed to emission from very high-order mX states [Figs. 1(b) and 1(c)]. Because of the m^2 and $\sim m^3$ scalings of $k_{m\mathrm{X},R}$ and $k_{m\mathrm{X},NR}$, these states can decay with lifetimes shorter than the pump-pulse width ($\tau_W \sim 50$ ps) and therefore can recycle more than once [ca. $(k_{m\mathrm{X},R} + k_{m\mathrm{X},NR})\tau_W$ times] with a nonzero $Q_{m\mathrm{X}}$ within one excitation cycle. The resulting enhancement of the contribution of mX's to PL can, in principle, lead to the observed upward turn.

In the second experiment, we extract the $Q_{2\mathrm{X}}/Q_{1\mathrm{X}}$ ratio from $g^{(2)}(\tau)$ measurements. $g^{(2)}(\tau)$ represents the probability distribution of time intervals between two sequential photon detection events. When one collects only emission from 1X states (e.g., by spectral selection, or in the cases where mX emission is suppressed), $g^{(2)}(\tau)$ exhibits an antibunching behavior for which the area of the $\tau = 0$ peak ($g_0^{(2)}$) is zero. However, $g_0^{(2)} > 0$ when the PL signal contains contributions from both 1X and 2X states. In the case of pulsed excitation, $g_0^{(2)}$, which corresponds to the probability of creating 2X and subsequent emission of two photons ($2\mathrm{X} \rightarrow 1\mathrm{X} \rightarrow 0$), scales in the lowest order as

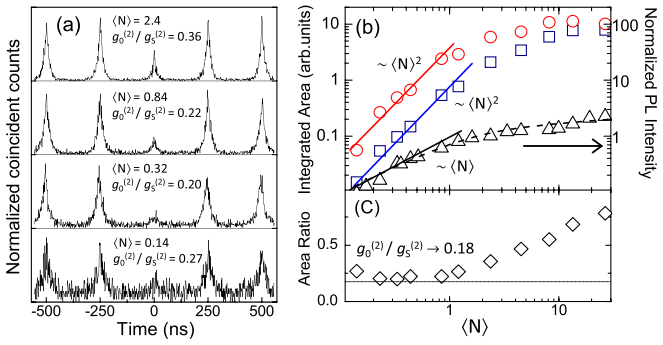

FIG. 2 (color online). (a). The $g^{(2)}$ measurements for a single 19-ML shell GNQD at different pump intensities. The zero-delay signal still persists at $\langle N\rangle < 1$. (b) Total PL (Δ) and time-integrated areas of $g_0^{(2)}$ ($\square$) and $g_s^{(2)}$($\bigcirc$) plotted as a function of $\langle N\rangle$. (c) Plot of $g_0^{(2)}/g_s^{(2)}$ vs $\langle N\rangle$ approaches 0.18 (solid line) as $\langle N\rangle \to 0$, in agreement with $Q_{2X} = 0.22 \pm 0.07$ obtained from the PL-saturation analysis [dashed line in (b)].

$\langle N\rangle^2$: $g_0^{(2)} \approx Q_{2X}Q_{1X}\langle N\rangle^2 + O(\langle N\rangle^3)$, where $O(\langle N\rangle^3)$ represents terms with order of $\langle N\rangle^3$ and higher. The area of the side peak measured at $\tau = T$ (T is the laser pulse period) ($g_s^{(2)}$) that reflects the probability of creation and emission of 1X in two successive excitation events also scales as $\langle N\rangle^2$: $g_s^{(2)} \approx (Q_{1X}\langle N\rangle)^2 + O(\langle N\rangle^3)$. Because of these scalings, $g_0^{(2)}/g_s^{(2)}$ approaches the value of Q_{2X}/Q_{1X} in the limit of $\langle N\rangle \to 0$ [21].

The $g^{(2)}$ measurements were conducted on the same individual GNQDs that were previously investigated using PL saturation. The $g^{(2)}$ traces of the 19-ML dots clearly show the persistence of the zero-delay peak in the $\langle N\rangle \to 0$ limit [Fig. 2(a)]. Further, the data reveal a clear $\langle N\rangle^2$ scaling of $g_0^{(2)}$ and $g_s^{(2)}$ [Fig. 2(b)]. More importantly, as $\langle N\rangle \to 0$, $g_0^{(2)}/g_s^{(2)}$ approaches 0.18 [Fig. 2(c)], in agreement with $Q_{2X} = 0.22 \pm 0.07$ derived from the PL-saturation studies [Fig. 2(b)]. Additional data indicating good agreement between the two approaches are shown in Fig. 3. Well resolvable zero-delay features are found for $g^{(2)}$ traces when $\langle N\rangle < 1$ [Figs. 3(a)–3(c)]. As $\langle N\rangle \to 0$, the $g_0^{(2)}/g_s^{(2)}$ values approach 0.60 (see supplemental material [23] for distinguishing single NQDs from NQD clusters), 0.32, and 0.03 in agreement with Q_{2X} of 0.55 ± 0.07, 0.28 ± 0.05, and <0.05 from the PL-saturation analysis. In Fig. 4(a), we plot the Q_{2X} derived from PL-saturation studies versus the Q_{2X}/Q_{1X} ratios measured by photon correlation for 13 NQDs (13- to 19-ML shells). Grouping of data points around the 45-degree line indicates a near-perfect agreement between both measurements.

In our PL-saturation analysis, we assumed $Q_{1X} = 1$. In order to understand how the deviation of Q_{1X} from unity affects the accuracy of derived Q_{2X}'s, we have simulated 2X QYs for three Q_{1X} values of 0.8, 0.5, and 0.3 and plotted them in Fig. 4(a) as a function of $g_0^{(2)}/g_s^{(2)}$, which is assumed to be a true measure of Q_{2X}/Q_{1X}. The simulated

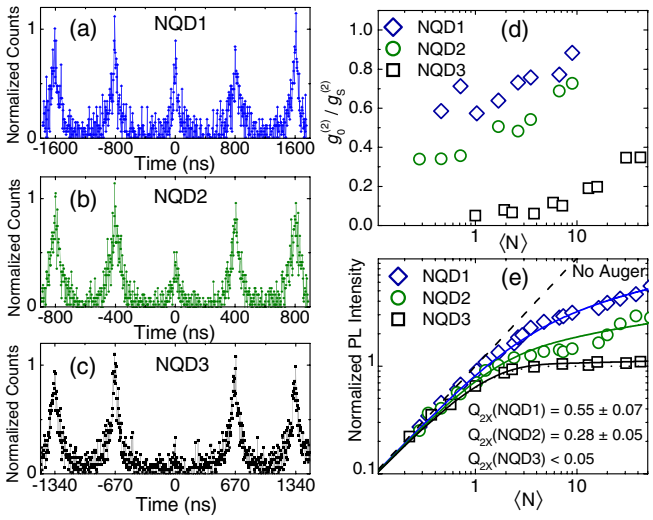

FIG. 3 (color online). (a)–(c) $g^{(2)}$ traces measured at $\langle N\rangle =$ 0.46, 0.34, and 1 for NQD 1, 2, and 3, respectively. NQD1 and NQD2 have the shell thickness of 19 MLs and NQD3 has a 16-ML-thick shell. (d) The plot of $g_0^{(2)}/g_s^{(2)}$ vs $\langle N\rangle$ gives $g_0^{(2)}/g_s^{(2)}$ of 0.60 (NQD1), 0.32 (NQD2), and 0.03 (NQD3) as the $\langle N\rangle \to 0$. (e) The PL intensity saturation analysis for the same set of the NQDs yields Q_{2X} of 0.55 ± 0.07, 0.28 ± 0.05, and <0.05, respectively.

data show that while in the regime of low $Q_{2X}/Q_{1X} < 0.3$ the PL-saturation approach provides an accurate measure of Q_{2X}/Q_{1X} irrespective of Q_{1X}, a systematic error increases with increasing Q_{2X}/Q_{1X}. However, the fact that the data points for the GNQDs with the highest Q_{2X}/Q_{1X} ratios are best described by calculations with Q_{1X} of 0.8 to 1 confirms our assumption of Q_{1X} being close to unity [23].

In Fig. 4(b), we plot a collection of the Q_{2X}'s obtained from more than 50 different NQDs via the PL-saturation measurement (open data points) and their average values

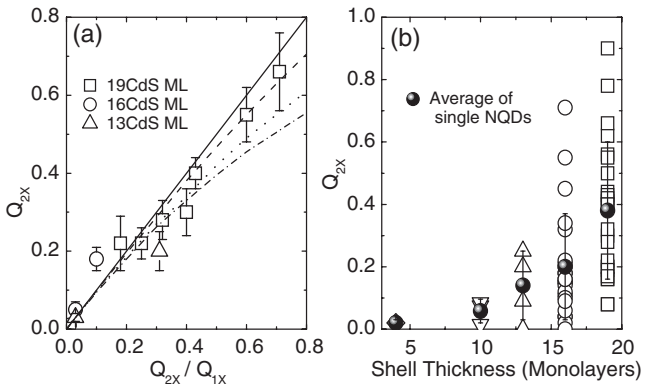

FIG. 4. (a) A plot of the Q_{2X} vs Q_{2X}/Q_{1X} for 13 different single GNQDs. Solid, dashed, dotted, and dash-dotted traces represent the simulations of Q_{2X} for the "PL-saturation" model for Q_{1X} of 1.0, 0.8, 0.5, and 0.3, respectively. (b) Q_{2X} obtained from the "PL-saturation" model for >50 individual NQDs (open symbols); average Q_{2X} for a given shell thickness are shown by solid circles.

(solid circles) as a function of shell thickness. These results show a consistent increase of Q_{2X} with increasing shell thickness with values for some 19-ML dots approaching a near-perfect Q_{2X} of ~0.9. However, we also observe a wide variation of Q_{2X} values ranging from <0.1 to ~0.9 with an average of 0.38 for nominally identical dots. This spread indicates a wide variation of 2X Auger lifetimes (1.4–77.0 ns). Since this large spread is observed for dots with a nominally identical shell thickness, it indicates that factors other than the core and the shell size may also influence Q_{2X}. One such factor is the structure of the core-shell interface affecting the shape of the confinement potential and consequently the rate of Auger recombination as was proposed by Cragg and Efros [25] and studied experimentally by García-Santamaría *et al.* [18].

The observed wide variation in 2X Auger time constants further suggests the existence of similarly wide variation of lifetimes of charged exciton (trions) because they are dependent on the same Auger process. Since the trions have been often invoked in various PL blinking models of standard NQDs [26,27], one might expect that the observed spread in the degree of Auger decay suppression could have an effect on PL fluctuation behaviors in GNQDs. However, our studies of PL time trajectories of more than 40 thick-shell (16- and 19-ML) dots show that all of them exhibit blinking-free PL (with nearly shot-noise limited photon-count-rate fluctuations independent of pump fluence) despite a wide variation in the Q_{2X} values (see supplemental material [23], Fig. S6). This observation suggests that the suppression of Auger recombination, which is required to obtain high QYs for 2X as well as trions, is not necessary to achieve complete suppression of PL intensity fluctuations. This further implies that blinking suppression in GNQDs results most likely from either suppression of photoionization or inhibition of random migration of long-lived charges generated by photoionization.

To summarize, we have studied Q_{2X}'s in individual GNQDs via two independent approaches and the results from both techniques are in excellent agreement. Our experiments reveal that it is possible to achieve a near-unity Q_{2X} in thick-shell GNQDs. For all samples, we observe significant dot-to-dot variations in Q_{2X}, which indicate that besides simple ''geometric'' factors (e.g., the core and the shell sizes), mX QYs strongly depend on more subtle structural features such as the internal shell structure and/or the properties of the core-shell interface. We also observe that suppression of PL intensity fluctuations in GNQDs does *not* require the suppression of Auger recombination, suggesting that a fluctuation-free behavior of PL in thick-shell CdSe/CdS GNQDs likely results from either suppression of photoionization or inhibition of random migration of long-lived charges if photoionization still takes place.

This work was conducted, in part, at the Center for Integrated Nanotechnologies (CINT), a U.S. Department of Energy (DOE), Office of Basic Energy Sciences (OBES) user facility. We acknowledge D. Werder for performing transmission electron microscopy studies. Y. P. is supported by CINT. Y. G., J. V., Y. C. acknowledge Los Alamos National Laboratory Directed Research and Development Funds. Work of A. V. M was supported by UT Dallas start-up funds. V. I. K. is supported by the Center for Advanced Solar Photophysics, an Energy Frontier Research Center of the OBES, Office of Science (OS), U.S. DOE. F. G. is supported by the Chemical Sciences, Biosciences and Geosciences Division of OBES, U.S. DOE. H. H. and J. A. H. acknowledge a Single Investigator Small Group Research Grant (2009LANL1096), OBES, OS, U.S. DOE.

*Present address: Department of Chemistry, Iowa State University, Ames, Iowa 50010, USA.
†Present address: Life Technologies, Inc., 29851 Willow Creek Road, Eugene, Oregon 97402, USA.
‡Present address: General Electric–Global Research Center 1, Research Circle, Niskayuna, New York 12309, USA.
§Corresponding author.
klimov@lanl.gov
‖Corresponding author.
htoon@lanl.gov

[1] R. Xie *et al.*, J. Am. Chem. Soc. **127**, 7480 (2005).
[2] J. McBride *et al.*, Nano Lett. **6**, 1496 (2006).
[3] B. Fisher *et al.*, Phys. Rev. Lett. **94**, 087403 (2005).
[4] V. I. Klimov *et al.*, Science **287**, 1011 (2000).
[5] L.-W. Wang *et al.*, Phys. Rev. Lett. **91**, 056404 (2003).
[6] V. I. Klimov *et al.*, Science **290**, 314 (2000).
[7] A. Muller *et al.*, Phys. Rev. Lett. **103**, 217402 (2009).
[8] R. M. Stevenson *et al.*, Nature (London) **439**, 179 (2006).
[9] H. Htoon *et al.*, Phys. Rev. Lett. **91**, 227401 (2003).
[10] I. Robel *et al.*, Nano Lett. **6**, 1344 (2006).
[11] J. Nanda *et al.*, J. Appl. Phys. **99**, 034 309 (2006).
[12] X. Wang *et al.*, Nature (London) **459**, 686 (2009).
[13] R. Osovsky *et al.*, Phys. Rev. Lett. **102**, 197401 (2009).
[14] Y. Chen *et al.*, J. Am. Chem. Soc. **130**, 5026 (2008).
[15] B. Mahler *et al.*, Nature Mater. **7**, 659 (2008).
[16] J. Vela *et al.*, J. Biophotonics **3**, 706 (2010).
[17] F. García-Santamaría *et al.*, Nano Lett. **9**, 3482 (2009).
[18] F. García-Santamaría *et al.*, Nano Lett. **11**, 687 (2011).
[19] P. Spinicelli *et al.*, Phys. Rev. Lett. **102**, 136801 (2009).
[20] H. Htoon *et al.*, Nano Lett. **10**, 2401 (2010).
[21] G. Nair, J. Zhao, and M. G. Bawendi, Nano Lett. **11**, 1136 (2011).
[22] V. I. Klimov, J. Phys. Chem. B **104**, 6112 (2000).
[23] See supplemental material at http://link.aps.org/supplemental/10.1103/PhysRevLett.106.187401 for the estimation of NQD absorption cross sections, the implications of a nonunity Q_{1X}, a $g^{(2)}$ measurement of NQD clusters, and blinkingfree emission.
[24] J. A. McGuire *et al.*, Acc. Chem. Res. **41**, 1810 (2008).
[25] G. E. Cragg and A. L. Efros, Nano Lett. **10**, 313 (2010).
[26] A. L. Efros and M. Rosen, Phys. Rev. Lett. **78**, 1110 (1997).
[27] K. Zhang *et al.*, Nano Lett. **6**, 843 (2006).